Available online at www.sciencedirect.com
ScienceDirect
International Journal of Heat and Fluid Flow 28 (2007) 1418–1428
International Journal of HEAT AND FLUID FLOW
www.elsevier.com/locate/ijhff

Flow produced in a conical container by a rotating endwall

M.P. Escudier *, J. O'Leary, R.J. Poole

Department of Engineering, University of Liverpool, Brownlow Street, Liverpool L69 3GH, United Kingdom

Received 5 October 2006; received in revised form 16 April 2007; accepted 18 April 2007
Available online 13 June 2007

Abstract

Numerical calculations have been carried out for flow in a truncated cone generated by rotation of one endwall. For both convergent (radius increasing with approach to the rotating endwall) and divergent geometries, vortex breakdown is suppressed beyond a certain angle of inclination of the sidewall. At the same time Moffat eddies of increasing strength and extent appear in the corner between the sidewall and the non-rotating endwall. For the divergent geometry, a zone of recirculation appears on the sidewall and eventually merges with the Moffat eddies. The flow phenomena identified from streamline patterns are consistent with the calculated variation of pressure around the periphery of the computational domain.

Keywords: Vortex breakdown; Conical container; Rotating endwall

1. Introduction

Rotation of one endwall of a closed cylinder completely filled with a fluid produces a wide range of flows from unremarkable steady swirling recirculation to a flow with up to three separate zones of embedded recirculation (vortex breakdowns) centred on the cylinder axis, to periodic time-varying flows and eventually to a fully turbulent flow. The flow structure is determined by two global parameters: the rotational Reynolds number, $Re = \Omega R^2/\upsilon$, and the aspect ratio of the cylinder, H/R. Ω is the angular velocity of the rotating endwall and R its radius, H is the cylinder height and υ is the kinematic viscosity of the fluid. Vogel's (1968) flow-visualisation experiments revealed the presence of a single region of recirculation for $1000 < Re < 2870$ and $1.39 < H/R < 2.12$ whereas a more complete picture, also based upon flow visualisation, was given by Escudier (1984) who extended the upper limits of the parameter ranges to $Re \approx 3480$ and $H/R \approx 3.65$. Since that time a number of studies have involved the investigation of flows in closely related geometries. Pereira and Sousa (1999) modified the experimental configuration to include a conical rotating endwall, Fujimura et al. (2004) investigated the flow generated by rotation of both endwalls, while Spohn et al. (1998) carried out experiments on flows with a free surface. Bühler (1985) reported on experiments for the flow in the gap between two concentric spheres, the outer of which was rotating, and on the flow in a conical container with curved endwalls, one of which was rotating (Bühler (1994)).

Given the combination of these experiments with exceptionally well defined, quite simple boundary conditions and an extraordinarily complex flowfield, it is unsurprising that there have also been numerous numerical studies of the 'container with endwall rotation' problem. Of note are the early works of Lugt and Haussling (1982), which was limited to calculating the single recirculation bubble, and the detailed simulations of Lopez (1990) who was the first to calculate the full extent of the flows observed by Escudier. Only recently have the numerical investigations predicted phenomena not previously observed experimentally. For example, Tsitverblit and Kit (1996) and Mullin et al. (1998) investigated numerically the inclusion of a central circular cylinder and found it to have a relatively small

* Corresponding author. Fax: +44 151 7944848.
E-mail address: m.p.escudier@liv.ac.uk (M.P. Escudier).

0142-727X/$ - see front matter © 2007 Elsevier Inc. All rights reserved.
doi:10.1016/j.ijheatfluidflow.2007.04.018

Nomenclature

a, b, p	constants in accuracy estimation scheme	Re	Reynolds number $\Omega R^2/\upsilon$
C_P	coefficient of pressure	Re_{EQ}	Reynolds number $\Omega R_{EQ}^2/\upsilon$
H	height of conical container (m)	Re_M	Reynolds number $\Omega R_M^2/\upsilon$
p	static pressure (Pa)	u	flow velocity (m/s)
p_c	stagnation pressure at centre of non-rotating endwall (Pa)	x	distance along container axis from rotating disk (m)
p_{ref}	reference pressure (static pressure at centre of rotating endwall) (Pa)	X_S	non-dimensional distance along axis to first stagnation point
r	radius of container at distance x (m)	α	angle of inclination of container sidewall
R	radius of rotating endwall (m)	Δr	radial extent of computation cell (m)
R_{EQ}	volume equivalent radius $\sqrt{(R^2 - RH\tan\alpha + (H^2\tan^2\alpha)/3)}$ (m)	Δx	axial extent of computation cell (m)
		η	dynamic viscosity of fluid (Pa s)
		υ	kinematic viscosity of fluid (m^2/s)
R_M	mean radius of truncated cone $R - (H\tan\alpha)/2$ (m)	ρ	density of fluid (kg/m^3)
		Ω	angular velocity of rotating endwall (s^{-1})

effect on the appearance of a single recirculation bubble. In a more recent paper, Mullin et al. (2000) showed both experimentally and numerically that the recirculation bubble was strongly influenced by the introduction of a tapered centrebody, which could be stationary or rotating. They argued that the sign of the axial pressure gradient depended upon whether the centrebody diameter increased or decreased between the non-rotating and the rotating endwalls and whether it was stationary or rotating, and that these two influences had a strong influence on the magnitude of the breakdown region. A decreasing diameter led to an adverse pressure gradient when the inner cylinder was rotating and enlargement of the breakdown whereas an increasing diameter had the opposite effect. The effects were also reversed if the inner cylinder was stationary.

The investigation reported here is numerical and concerned with the flows produced in truncated conical containers by a rotating endwall (illustrated schematically in Fig. 1). The three global parameters required to characterise the problem are the Reynolds number $Re = \Omega R^2/\upsilon$, the aspect ratio H/R, and the slope angle of the inclined wall, α, taken as positive for the divergent geometry (radius r increasing with axial distance x from the rotating disk) and negative for the convergent geometry (r decreasing). Similarities are apparent between our geometries and the conical arrangement investigated by Bühler (1994) and also with the tapered centrebody geometries of Mullin et al. (2000) in the sense that the divergent geometry, $\alpha > 0°$, corresponds with Mullin et al.'s decreasing gap, while the convergent geometry, $\alpha < 0°$, corresponds with their increasing gap. An essential difference compared with the geometries investigated by Mullin et al., which precludes a direct comparison between our results and theirs, is that in the absence of a centrebody the no-slip condition is imposed only on the outer conical surface and the rotating endwall. As they showed, their results were critically dependent on whether the inner cylinder was rotating not simply upon area change. In addition to streamline patterns, we also present the pressure variation over the surface of the container to further explore the pressure-gradient arguments of Mullin et al.

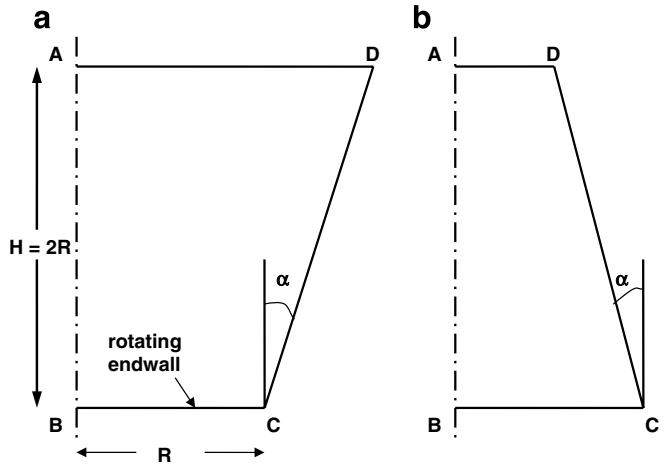

Fig. 1. Schematic of flow domain (a) divergent geometry, $\alpha > 0°$ and (b) convergent geometry, $\alpha < 0°$.

2. Numerical method

To compute the flow field within the rotating endwall conical container, discussed above, we make use of the assumption that the flow is laminar, incompressible, steady and axisymmetric (i.e. two-dimensional). The governing equations are then those expressing conservation of mass Eq. (1) and momentum Eq. (2):

$$\nabla \cdot u = 0, \tag{1}$$

$$\nabla \cdot (\rho u u) = -\nabla p + \eta \nabla \cdot \nabla u. \tag{2}$$

In these equations, u represents the vector velocity, p the static pressure, ρ the fluid density and η its dynamic viscosity. We used the commercial package FLUENT (version 6.0) to solve Eqs. (1) and (2). This well-established code has been used extensively in the calculation of complex flows (see Fellouah et al., 2006; Huang et al., 2006; Taha and Cui, 2006; Hu et al., 2005 for recent examples) and, with the correct implementation, is adequate to model the laminar flows under consideration here. We used the segregated solver in which the momentum and swirl velocity equations were discretised using a second-order upwinding scheme. Coupling of the pressure and velocity was achieved using the well-known SIMPLEC implementation of Van Doormal and Raithby (1984).

Double precision (14 d.p.) was used for all the calculations so that round-off errors are negligible. The iterations were terminated whenever the scaled residuals (see Celik and Li, 2005) for the solutions for the two components of velocity and the continuity equation approached an asymptotic value. In general the scaled residuals were observed to reach a level between 1×10^{-12} and 1×10^{-15}.

A preliminary series of calculations was carried out with 200×100, 400×200 and 800×400 uniform (i.e. $\Delta r=\Delta x$) cells for the base case ($\alpha=0°$) to investigate the accuracy of our simulations. Firstly we made a qualitative comparison between our calculated streamlines and the experimental visualisations of Escudier (1984). Such a comparison is shown in Fig. 2 for the particularly complex case of a double breakdown. As can be seen the simulation predicts both the occurrence of the primary and secondary recirculation bubbles as well as their size and location along the centreline. In addition to this qualitative comparison, our consistent mesh-refinement procedure allows us to undertake a more quantitative validation and to directly estimate the numerical accuracy of our simulations. A sensitive criterion to determine this accuracy is the axial distance from the non-rotating endwall to the location along the centreline of the first stagnation point, non-dimensionalised by the disk radius, which we choose here to define X_S. The variation of this quantity with increasing mesh refinement is shown in Fig. 3. Firstly we note that the *variation* of X_S between meshes is about 1% at most and so can be regarded as negligibly small. Secondly, fitting these points to an equation of the form $a(\Delta r)^p+b$ allows us to estimate the order of accuracy (p) of our simulations (Ferziger and Peric, 2001). Although our simulations are nominally sec-

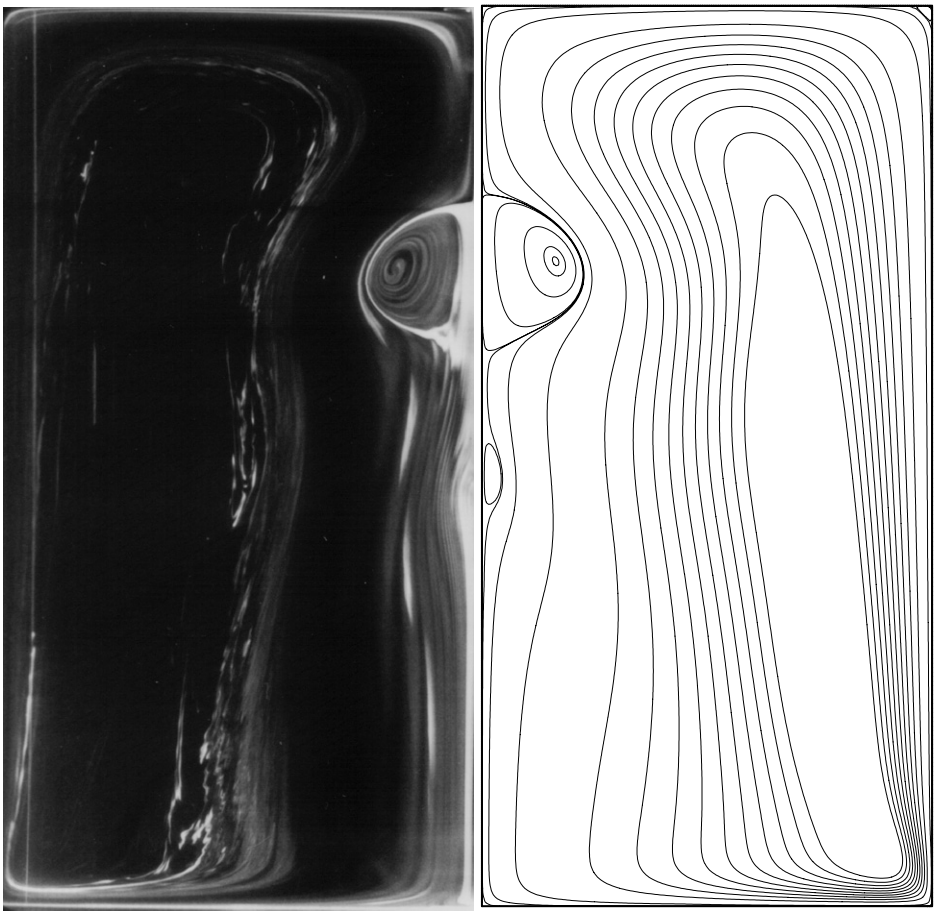

Fig. 2. Comparison of computed streamlines and experimental flow visualisation (taken from Escudier, 1984) of flow produced in a cylindrical container, $Re=1854$, $H/R=2$ (Mesh M2).

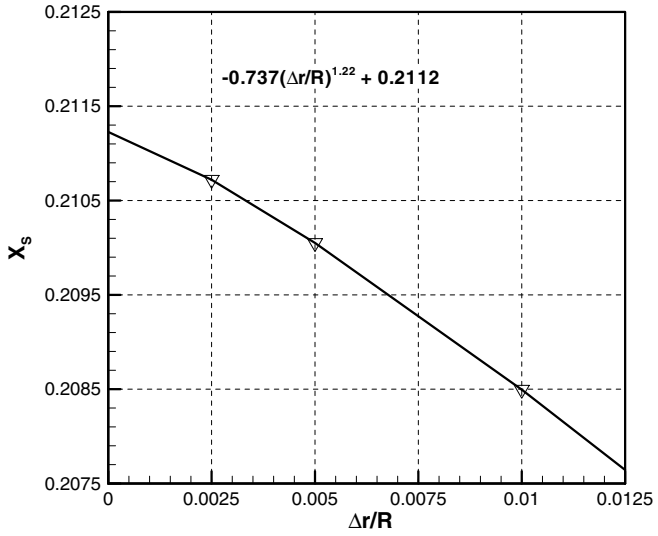

Fig. 3. Variation of non-dimensional distance to stagnation point X_S with mesh refinement for base case ($\alpha = 0°$).

Table 1
Mesh characteristics for base case together with estimates of numerical accuracy

Mesh ($\alpha = 0°$)	NC	X_S	% error in X_S
M1	20000	0.2085	1.31
M2	80000	0.2101	0.56
M3	320000	0.2107	0.24
Richardson extrapolation		0.2112	0.00

ond order in accuracy, we note that they are in reality only slightly better than first order ($p = 1.2$). However if we use this order to estimate the 'Richardson' extrapolation value for this quantity (i.e. the value extrapolated to zero mesh size), shown in Table 1, we still find that the error in our simulations is negligibly small.

On the basis of this analysis of the mesh dependency, all subsequent calculations were carried out with a nominal 400×200 (i.e. 80000) cells. The actual number of cells (NC) used was determined by the geometry under consideration since the smaller computational domain of the convergent geometry ($\alpha < 0°$) required fewer cells whereas the divergent geometry ($\alpha > 0°$) required more. In addition, a finer mesh was used in the corner between the inclined sidewall and the non-rotating endwall to resolve the small-scale flow structure as discussed below. Sahin and Owens (2003), who investigated the two-dimensional, lid-driven cavity flow discuss in some detail numerical problems arising from the singularities which arise in the corners between the sliding lid and the stationary cavity walls and the measures implemented to overcome them. In our case, a similar singularity occurs at the corner between the rotating disk and the container sidewalls but no special measures were needed to address numerical problems.

The main parameter varied in the calculations was the cone angle α. Calculations were carried out for α between $+25°$ and the limiting case of $-26.6°$ while the aspect ratio was fixed at $H/R = 2$. For the majority of calculations the Reynolds number chosen was 1854 with a few additional calculations carried out for 2354 and 3354. The lower Reynolds number corresponds to a condition just within the base-case (i.e. $\alpha = 0°$) boundary for which Escudier (1984) found a double breakdown whereas the higher Reynolds number is just above the boundary and corresponds to a single breakdown.

3. Results of numerical calculations

3.1. Streamline patterns for the convergent geometry

As is immediately apparent from Fig. 4, for $Re = 1854$, breakdown is suppressed for α between $-7°$ and $-8°$ although even for the limiting case of $\alpha = -26.6°$ a slight bulge is still evident in the streamlines in the vicinity of the breakdowns which occur for $\alpha > -8°$. The bulge moves progressively along the axis, towards the rotating disk, as $|\alpha|$ increases. If we regard the geometry with $\alpha < 0°$ as corresponding to gap width increasing towards the rotating end, then this behaviour is qualitatively similar to what was found by Mullin et al. (2000) when the inner cylinder was not rotating.

A feature not remarked upon hitherto in investigations of the container problem is the appearance of a Moffat corner-eddy system (Moffat, 1964) in the corner between the sidewall and the non-rotating endwall. Such eddies have been observed in a number of other geometries involving rotating surfaces including the concentric-cone arrangement investigated by Hall et al. (2007). This omission for the container problem is surprising because the existence of such vortices might have been anticipated. In fact, careful scrutiny of streamline patterns reported in several earlier papers (e.g. Lugt and Haussling, 1982; Bhattacharya and Pal, 1998; Brons et al., 1999) hints at their presence though it may be that the earlier calculations were performed with grids too coarse to confirm the occurrence of Moffat vortices. The analytical approach adopted by Hall et al. (2007) reveals the first four of an infinite sequence of counter-rotating toroidal eddies as the apex of their cones is approached. As can be seen in Fig. 4, the scale and penetration of the Moffat eddies increases with increasing values of $|\alpha|$ but it is clear that a Moffat eddy is present for all values of α, including 0°.

For the higher Reynolds number of 2354, shown in Fig. 5, the streamlines are qualitatively similar to those for $Re = 1854$. Breakdown is suppressed for $\alpha < -12°$ compared with $-8°$ for the lower Re value while the Moffat eddies appear more pronounced at about the same inclination angle.

3.2. Streamline patterns for the divergent geometry, $\alpha > 0°$

The flow behaviour for $\alpha > 0°$ as revealed in Fig. 6 is somewhat more complex than for the convergent cases. The breakdown is again gradually suppressed as α

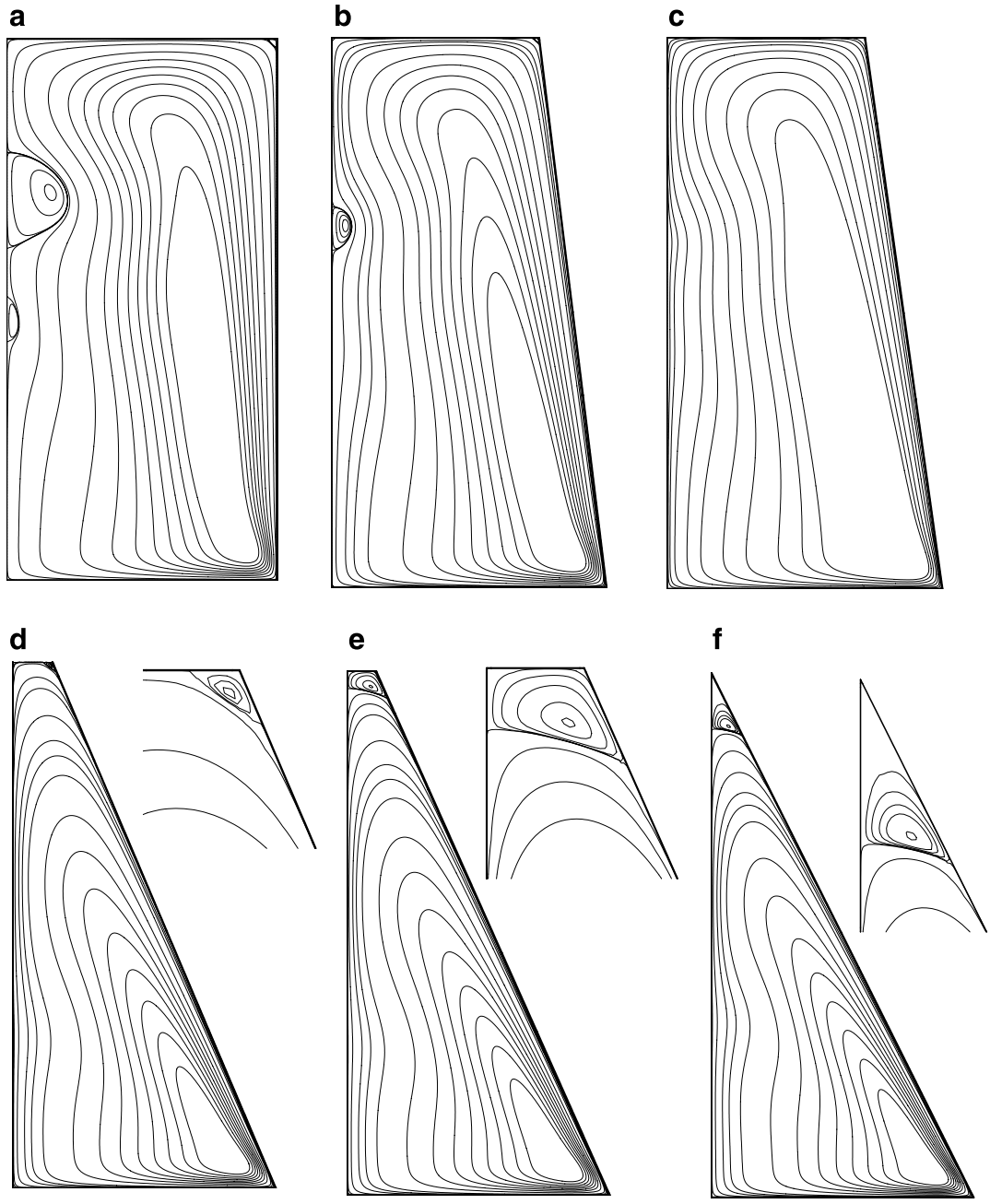

Fig. 4. Streamlines for convergent geometry with $Re = 1854$, (a) $\alpha = 0°$, (b) $\alpha = -7°$, (c) $\alpha = -8°$, (d) $\alpha = -23°$, (e) $\alpha = -24°$ and (f) $\alpha = -26.6°$.

increases but for $Re = 1854$ is still clearly evident for the highest inclination angle, 25°, and for α greater than 10° Moffat eddies appear in the upper corner formed between the inclined sidewall and the non-rotating endwall. For $\alpha = 20°$ a second Moffat eddy is just detectable and for $\alpha = 25°$ is very well resolved by the calculation. Another prominent feature of the calculations is the toroidal "blister" of recirculation which appears high up on the inclined sidewall for $\alpha > 20°$. As we shall see from calculations of the pressure distribution, this separation bubble is associated with the occurrence of a positive pressure gradient on the inclined wall. One of the cases reported by Hall et al. (2007) for their concentric-cone geometry also reveals a zone of recirculation on the outer cone wall for the situation where the cones are contra rotating while the spherical lid rotates in the same sense as the inner cylinder.

From Fig. 7 it is seen that at the higher Reynolds number of 2354 breakdown on the axis is completely suppressed for $\alpha > 10°$ although the near-axis streamlines remain highly distorted even for the highest inclination angle. Moffat eddies are easily seen even for $\alpha = 5°$, the onset of sidewall separation is just apparent for $\alpha = 20°$, and by 25° has grown considerably and is on the verge of merging with the Moffat eddies. For the final calculation, the results of which are shown in Fig. 8, with $\alpha = 25°$ and $Re = 3354$,

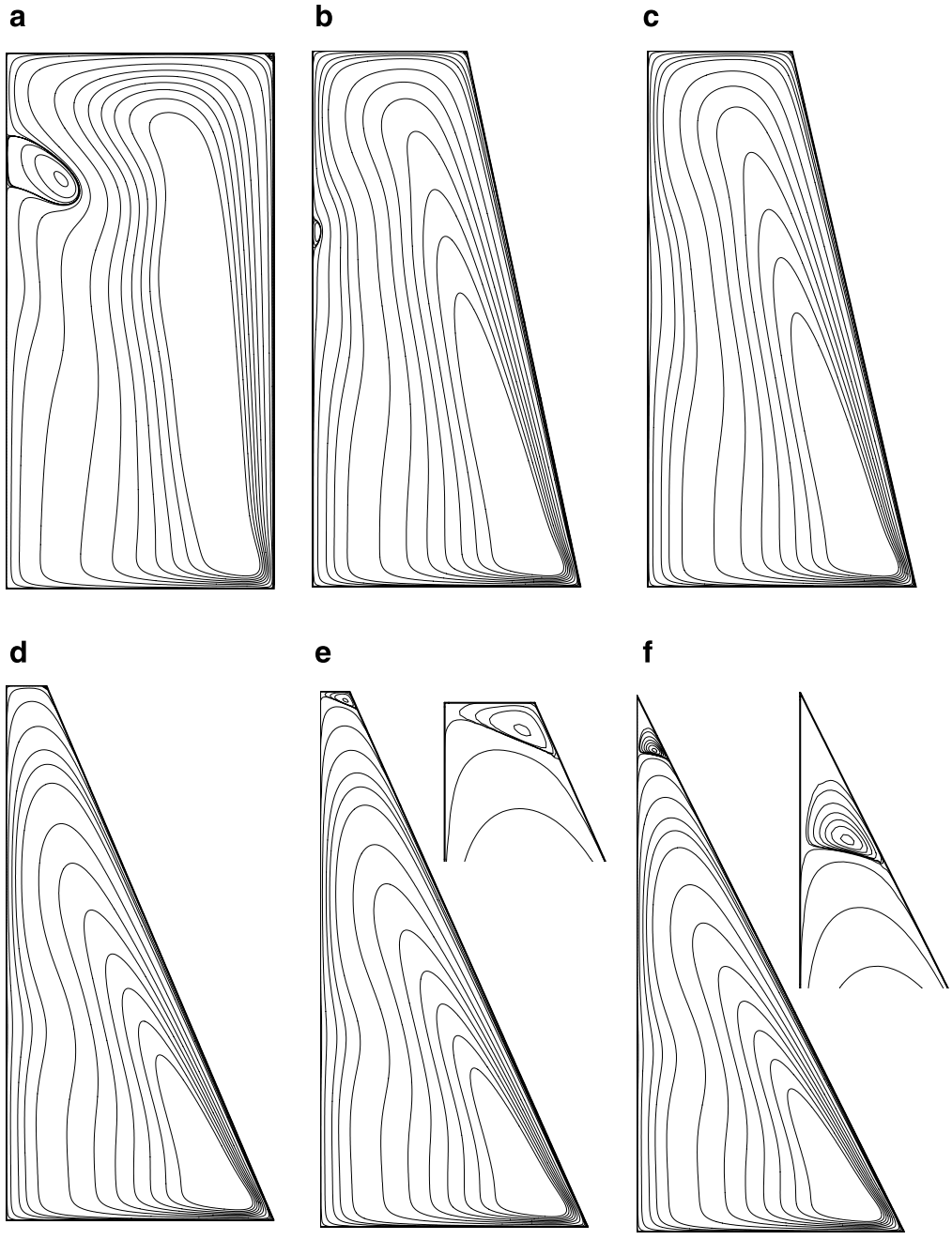

Fig. 5. Streamlines for convergent geometry with $Re = 2354$, (a) $\alpha = 0°$, (b) $\alpha = -12°$, (c) $\alpha = -13°$, (d) $\alpha = -23°$, (e) $\alpha = -24°$ and (f) $\alpha = -26.6°$.

the Moffat eddy system has indeed merged with the inclined-wall recirculation bubble. For this Reynolds number, as shown by the experiments of Escudier (1984), there is no breakdown even for the base case, $\alpha = 0°$ and it is likely that in reality the flow would be unsteady.

The calculations presented in this paper are all for the same value of an aspect ratio defined as H/R. It might be thought that a more appropriate measure of the aspect ratio would be one defined in terms of either the mean radius $R_M = R - (H\tan\alpha)/2$ or a volume-equivalent radius $R_{EQ} = \sqrt{(R^2 - RH\tan\alpha + (H^2\tan^2\alpha)/3)}$. It has been suggested that the boundaries for the occurrence of vortex breakdown in terms, of H/R_M or H/R_{EQ} versus Reynolds number (defined as either $Re = \Omega R^2/\upsilon$, $Re_M = \Omega R_M^2/\upsilon$ or $Re_{EQ} = \Omega R_{EQ}^2/\upsilon$) might correspond to the boundaries for flow in a cylindrical container, as identified experimentally by Escudier (1984). To explore this possibility, in Fig. 9 we have plotted points corresponding to the numerical calculations presented in this paper using the volume-equivalent radius R_{EQ} in the definitions of both the aspect ratio and the Reynolds number (thin *curves*). Also shown (along the horizontal broken lines) are points in which H/R has been modified but not Re. A similar plot based on R_M for the characteristic radius led to very small differences and is not shown here.

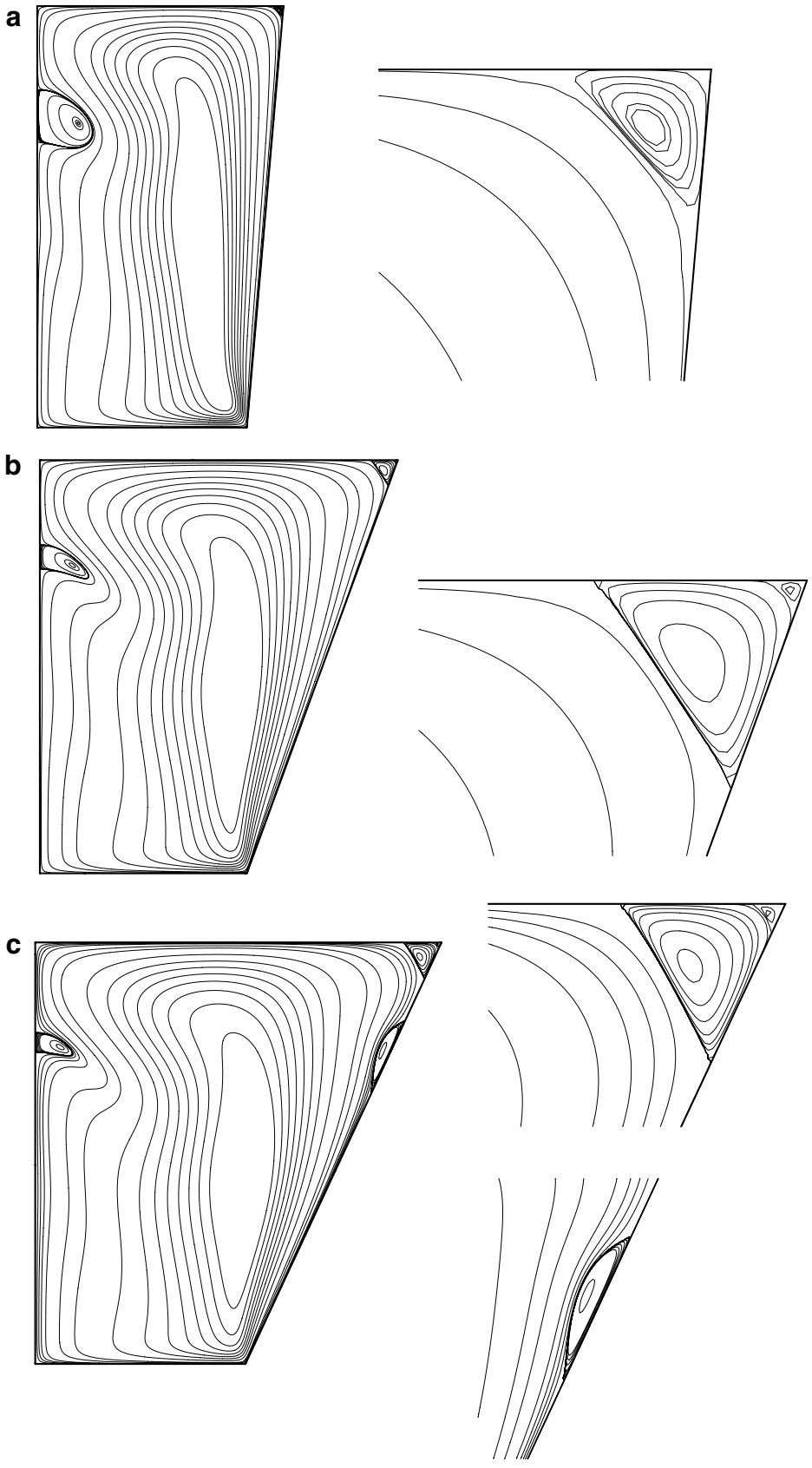

Fig. 6. Streamlines for divergent geometry with $Re = 1854$, (a) $\alpha = 5°$, (b) $\alpha = 20°$ and (c) $\alpha = 25°$.

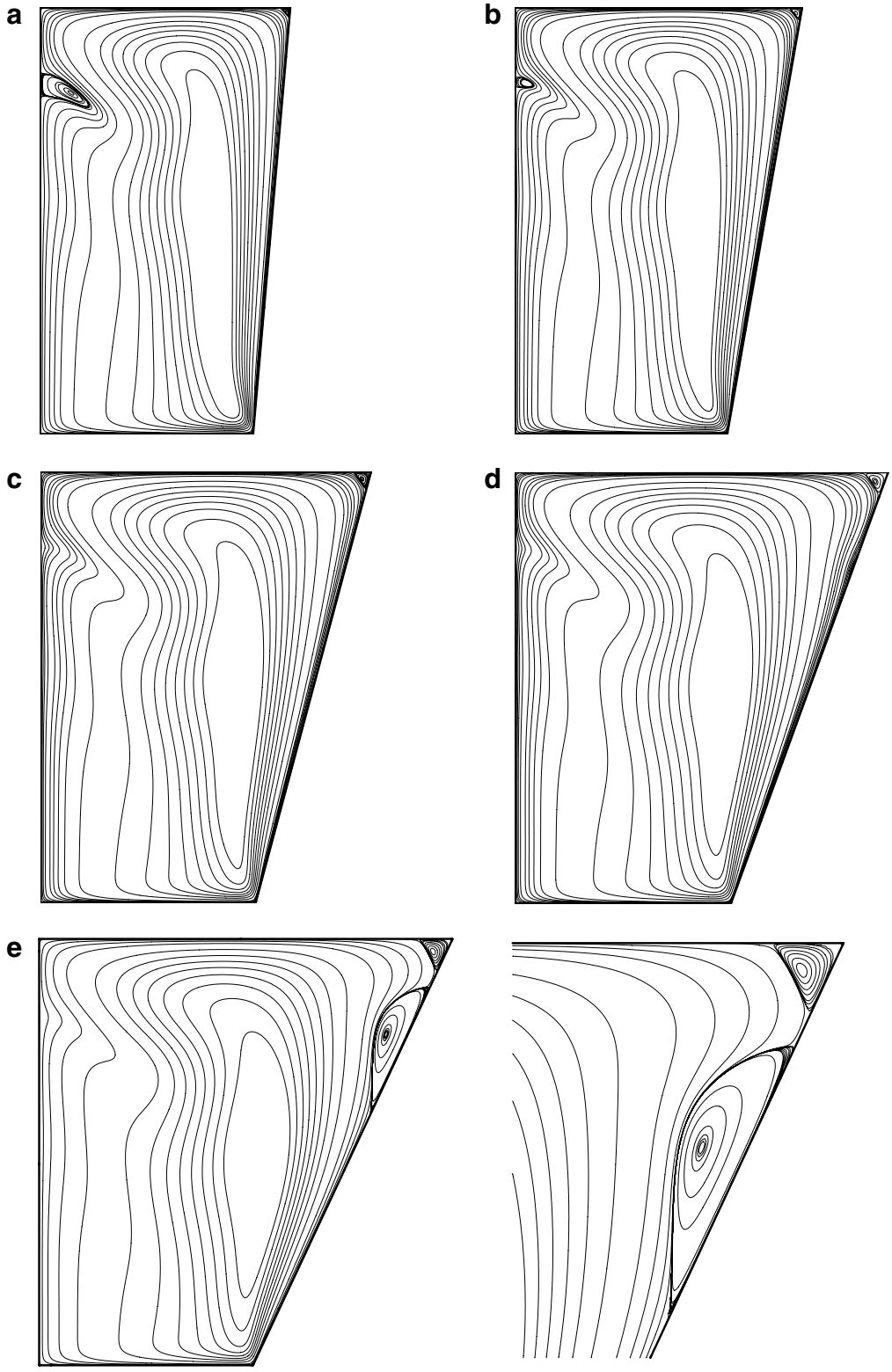

Fig. 7. Streamlines for divergent geometry with $Re = 2354$, (a) $\alpha = 5°$, (b) $\alpha = 10°$, (c) $\alpha = 15°$, (d) $\alpha = 20°$ and (e) $\alpha = 25°$.

For $Re = 1854$, the closed points Fig. 9 correspond to $\alpha = 25°$, 20°, 5°, 0° and −7°, while the open points correspond to −8°, −23°, −24° and −26.6°. For $Re = 2354$, the open points to the left correspond to $\alpha = 25°$, 20° and 15°, those to the right correspond to −13°, −23°, −24° and −26.6° while the closed points correspond to 10°, 5° and −12°. It is clear that the proposed criterion fails for about one third of the cases considered here (some points lie outside the range of the graph), both in terms of "predicting" breakdown where it does not occur and not

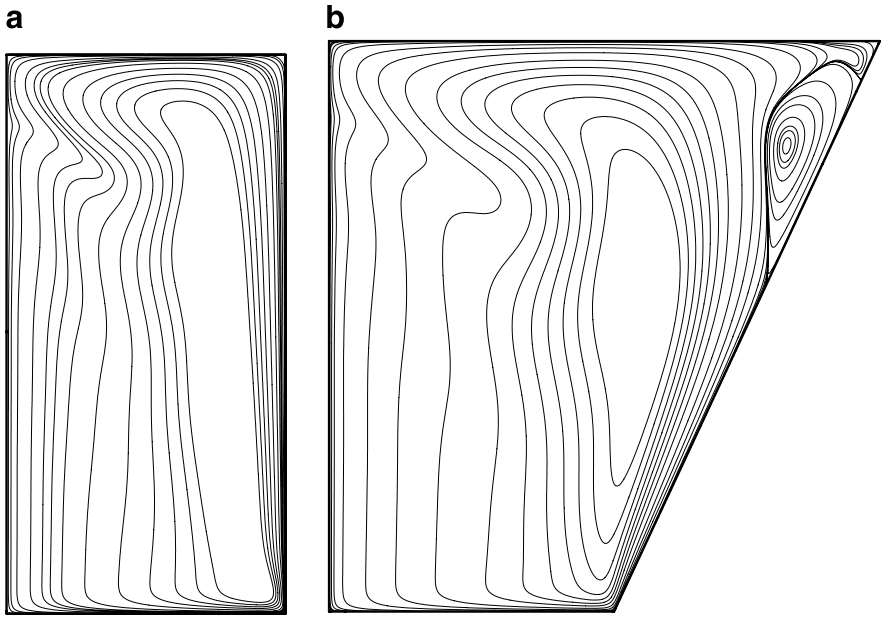

Fig. 8. Streamlines for divergent geometry with $Re = 3354$, (a) $\alpha = 0°$ and (b) $\alpha = 25°$.

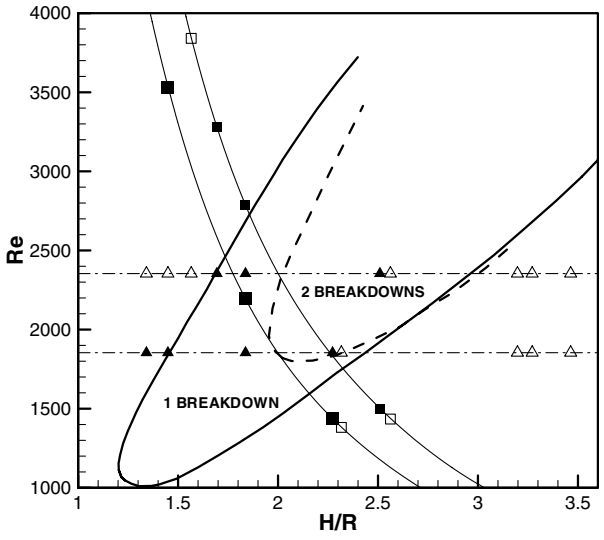

Fig. 9. Closed symbols, ■ and ▲, correspond to vortex breakdown according to the numerical calculations; open symbols, □ and △, to the absence of breakdown. The thick curves correspond to the boundaries established experimentally by Escudier (1984).

predicting it where it does. More specifically, at the lower Reynolds number the criterion predicts breakdown for $\alpha = 25°$ where none is observed but not for $-8°$ where it is (in fact the latter case falls on the one/two breakdown boundary). For the higher Reynolds number, the criterion works well for $\alpha > 0°$ but fails badly for $\alpha = -13°$ where no breakdown is predicted while in practice this is well within the boundary for two breakdowns to occur.

The motivation for defining an effective radius was the possibility that the effect of sidewall inclination could be explained in terms of a modified aspect ratio. Although the explanation is not fully supported by our calculations, it could be argued that the general trend indicated by the points in Fig. 9 suggests that part of the influence of the inclined sidewalls is an effective change in aspect ratio. The breakdown criterion is in better agreement with the calculations if only H/R is modified.

3.3. Wall pressure distribution

Mullin et al. (2000) demonstrated that for their geometry enlargement or suppression of vortex breakdown on the surface of the central conical rod which they investigated was associated with a pressure gradient brought about by convergence or divergence of the annular gap and rotation or non-rotation of the rod. When the inner cylinder was rotating and tapered towards the rotating cylinder, an adverse pressure gradient was generated which enhanced the breakdown region whereas breakdown was diminished when the inner cylinder increased in diameter. The trends were reversed in the absence of rotation. As we have already commented, although there is clearly an association between area change and changes in breakdown structure in our calculations, there are essential differences between our work and that of Mullin et al. as a consequence of the absence of a centrebody to provide a no-slip boundary condition for our problem so direct comparisons cannot be made.

The variation of the pressure coefficient, $C_P \equiv 2(p - p_{ref})/\rho\Omega^2R^2$, with distance s around the periphery of a central plane is shown in Figs. 10–12. The reference pressure p_{ref} has been taken as the pressure at the centre of the rotating disk (i.e. location **B** in Fig. 1). Fig. 10 shows the variation of C_P from the centre of the non-rotating endwall (**A**), down the axis to the rotating disk (**B**), and part way across the rotating disk. The curves are shown for 5° inter-

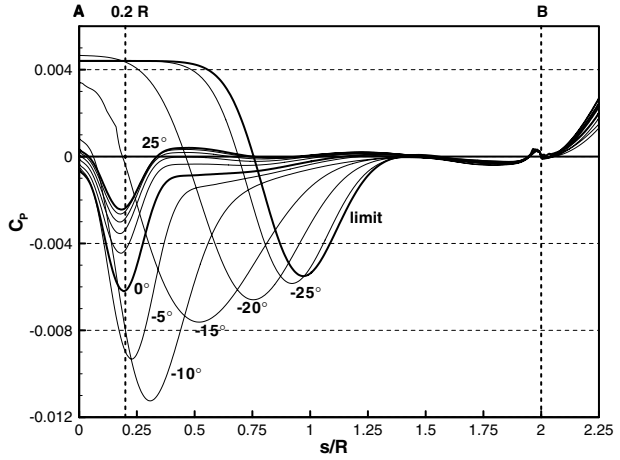

Fig. 10. Variation of pressure coefficient around domain boundary for $0 < s < 2.25R$. The curves correspond to 5° intervals in the inclination angle α plus the limiting case.

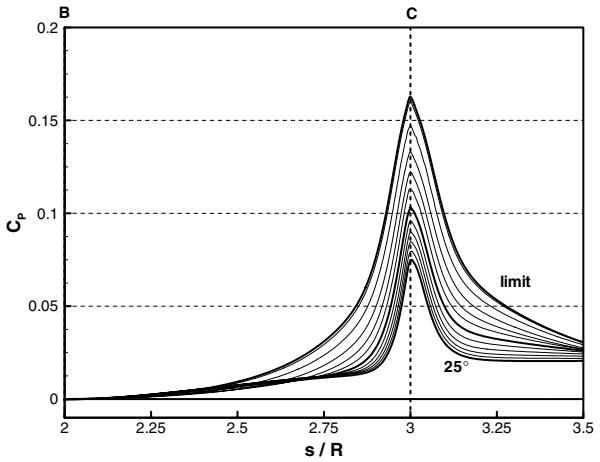

Fig. 11. Variation of pressure coefficient across rotating endwall and part way along inclined sidewall.

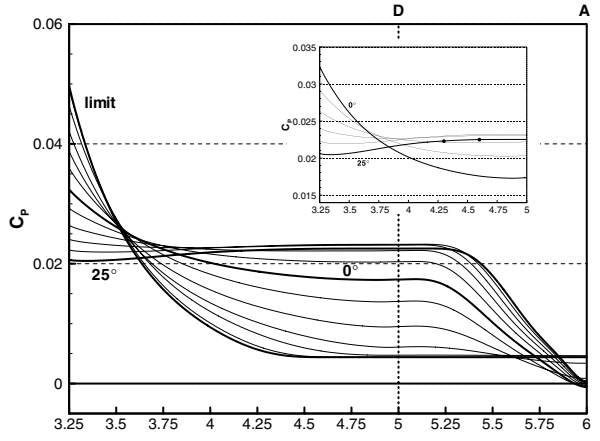

Fig. 12. Variation of pressure coefficient along inclined sidewall and across non-rotating endwall. The non-dimensional distance from **C** to **D** has been scaled to range from 3 to 5 and that from **D** to **A** to range from 5 to 6.

vals in α from $+25°$ to $-25°$ plus the limiting case ($-26.6°$). In this figure the distance s has been normalised with the radius R. Although it is the pumping action of the rotating disk which produces flow within the container, in fact the pressure difference $(p_c - p_{ref})$, p_c being the stagnation pressure at the centre of the non-rotating disk (**A**), is negative for $15° > \alpha > -5°$ and only becomes positive for $\alpha > 15°$ and $\alpha < -5°$. For the divergent geometry the pressure falls rapidly for $0 < s < 0.2R$ before increasing to an internal stagnation point (corresponding to the "nose" of the breakdown region) at about $0.4R$ where the C_P curves reveal a pronounced "knee". The changes for the convergent case are more complex and show a considerable pressure increase at **A** for $\alpha < -5°$ combined with a smoother recovery beyond the minimum. The absence of a well defined knee in the curve corresponds to the suppression of vortex breakdown for $\alpha < -5°$. For $1.4 < s/R < 2$, with approach to the spinning disk, the C_P curves for all inclination angles are practically indistinguishable.

The variation of C_P across the rotating endwall (**B** to **C**) and part way along the inclined sidewall is shown in Fig. 11 with s again scaled with R. The pressure increases to a peak at the periphery of the spinning disk, much as would be expected though the pressure levels for all cases are considerably below that for solid-body rotation (i.e. $C_P = (r/R)^2$). The monotonic changes in the peak and the curves generally suggest that as α decreases, the sidewalls increasingly act essentially as a blockage.

In the final figure showing the variation of C_P (Fig. 12), the distance along the domain boundary has been scaled to have the value 3 at location **C** (the edge of the rotating endwall), the value 5 and at location **D** and the value 6 at location **A**. Thus distance along **CD** has been scaled with its length $2R\sec\alpha$ and along **DA** with its length $R + 2R\operatorname{cosec}\alpha$. The effect of this normalisation is that the computational domain has been effectively transformed to a rectangle. The most significant feature of Fig. 12 is the change in pressure gradient from negative to positive (or favourable to adverse) on the inclined sidewall for α between 10° and 15°. For $\alpha = 25°$ the gradient is sufficiently adverse to cause the separation blister seen in Fig. 4. The two filled circles on the 25° curve in the larger scale insert in Fig. 12 delineate the extent of the blister.

4. Conclusions

The results of numerical calculations have been presented for the flow generated in a truncated cone by rotation of one endwall. For an aspect ratio $H/R = 2$ and a Reynolds number Re of 1854, the results show that vortex breakdown which occurs for the base case of a circular cylinder is suppressed if the angle of inclination of the conical sidewall α is less than $-7°$, for the convergent geometry, but is still present, although reduced in magnitude, for $\alpha = 25°$ for the divergent geometry. The results are qualitatively similar to those reported by Mullin et al. (2000) for a stationary inner cylinder. Moffat eddies are increasingly

prominent in the corner between the sidewall and the non-rotating endwall as the inclination angle is increased. For the divergent geometry with 25° inclination angle, a further region of recirculation appears about three quarters of the way along the sidewall as a result of the adverse pressure gradient which arises for $\alpha > 10°$. Qualitatively similar results are found at higher Reynolds numbers although the breakdown is also suppressed in the divergent geometry if $\alpha > 10°$ for $Re = 2354$, and for the combination $Re = 3354$ with $\alpha = 25°$ the Moffat eddies merge with the recirculation region. For some conditions, the calculations of Hall et al. (2007) reveal a similar recirculation blister on the outer wall of their concentric-cone geometry.

Acknowledgements

The authors thank Professor Manuel Alves, Faculdade de Engenharia Universidade do Porto, for advice regarding the estimation of the numerical accuracy of our simulations. We are also grateful to a referee for suggesting the use of a volume-equivalent or mean radius to explore the effect of aspect ratio on the occurrence of breakdown and to another referee for bringing two relevant references to our attention.

References

Bhattacharya, S., Pal, A., 1998. Axisymmetric vortex breakdown in a filled cylinder. Int. J. Eng. Sci. 36 (5/6), 555–563.

Brons, M., Voigt, L.K., Sorensen, J.K., 1999. Streamline topology of steady axisymmetric vortex breakdown in a cylinder with co- and counter-rotating end-covers. J. Fluid Mech. 401, 275–292.

Bühler, K., 1985. Strömungsmechanische Instabilitaeten zäher Medien im Kugelspalt, Fortschrittberichte VDI Reihe 7(96).

Bühler, K., 1994. Wirbelströmungen mit Rückströmgebiten. DGLR Jahrbuch II, 887–894.

Celik, I.B., Li, J., 2005. Assessment of numerical uncertainty for the calculations of turbulent flow over a backward-facing step. Int. J. Numer. Meth. Fluids 49 (9), 1015–1031.

Escudier, M.P., 1984. Observations of the flow produced in a cylindrical container by a rotating endwall. Exp. Fluids 2, 189–196.

Fellouah, H., Castelain, C., Ould El Moctar, A., Peerhossaini, H., 2006. A numerical study of Dean instability in non-Newtonian fluids. J. Fluids Eng. Trans. ASME 128, 34–41.

Ferziger, J.H., Peric, M., 2001. Computational Methods for Fluid Dynamics. Springer, New York.

Fujimura, K., Koyama, H.S., Hyun, J.M., 2004. An experimental study on vortex breakdown in a differentially-rotating cylindrical container. Exp. Fluids 36, 399–407.

Hall, O., Hills, C.P., Gilbert, A.D., 2007. Slow flow between concentric cones. Q. J. Mech. Appl. Math. 60 (1), 27–48.

Hu, L.Y., Zhou, L.X., Zhang, J., Shi, M.X., 2005. Studies on strongly swirling flows in the full space of a volute cyclone separator. AICHE J. 51 (3), 740–749.

Huang, Z., Olsen, J.A., Kerekes, R.J., Green, S.I., 2006. Numerical simulation of the flow around rows of cylinders. Comp. Fluids 35, 485–491.

Lopez, J.M., 1990. Axisymmetric vortex breakdown: Part 1. Confined swirling flow. J. Fluid Mech. 221, 533–552.

Lugt, H.J., Haussling, H.J., 1982. Axisymmetric vortex breakdown in rotating fluid within a container. Trans. ASME J. Appl. Mech. 49, 921–923.

Moffat, H.K., 1964. Viscous and resistive eddies near a sharp corner. J. Fluid Mech. 18, 1–18.

Mullin, T., Tavener, S.J., Cliffe, K.A., 1998. On the creation of stagnation points in a rotating flow. J. Fluids Eng. 120, 685–689.

Mullin, T., Kobine, J.J., Tavener, S.J., Cliffe, K.A., 2000. On the creation of stagnation points near straight and sloped walls. Phys. Fluids 12 (2), 425–431.

Pereira, J.C.F., Sousa, J.M.M., 1999. Confined vortex breakdown generated by a rotating cone. J. Fluid Mech. 385, 287–323.

Sahin, M., Owens, R.G., 2003. A novel fully implicit finite volume method applied to the lid-driven cavity problem – Part I: High Reynolds number flow calculations. Int. J. Numer. Meth. Fluids 42, 57–77.

Spohn, A., Mory, M., Hopfinger, E.J., 1998. Experiments on vortex breakdown in a confined flow generated by a rotating disc. J. Fluid Mech. 370, 73–99.

Taha, T., Cui, Z.F., 2006. CFD modeling of slug flow in vertical tubes. Chem. Eng. Sci. 61, 676–687.

Tsitverblit, N., Kit, E., 1996. Numerical study of axisymmetric vortex breakdown. Acta Mech. 118, 79–98.

Van Doormal, J.P., Raithby, G.D., 1984. Enhancements of the SIMPLE method for predicting incompressible fluid flows. Numer. Heat Transfer 7, 147–163.

Vogel, H.U., 1968. Experimentelle Ergebnisse über die laminare Strömung in einem zyindrischen Gehäuse mit darin rotierende Scheibe, MPI für Strömingsforschung, Bericht 6.